Advances in Geo-Energy Research

Vol. 15, No. 3, p. 230-244, 2025

Original article

Field-scale investigation of CO_2 plume dynamics under spatial wettability variations: Implications for geological CO_2 storage

Haiyang Zhang[1]*, Mohamed Mahmoud[2], Stefan Iglauer[3], Muhammad Arif[1]*

[1]*Department of Chemical & Petroleum Engineering, Khalifa University, Abu Dhabi 127788, United Arab Emirates*

[2]*Department of Petroleum Engineering, College of Petroleum Engineering & Geosciences, King Fahd University of Petroleum & Minerals, Dhahran 31261, Saudi Arabia*

[3]*Centre for Sustainable Energy and Resources, School of Engineering, Edith Cowan University, Joondalup, WA 6027, Australia*

Keywords:
Geological CO_2 storage
trapping capacity
plume migration
wettability heterogeneity
sustainability

Cited as:
Zhang, H., Mahmoud, M., Iglauer, S., Arif, M. Field-scale investigation of CO_2 plume dynamics under spatial wettability variations: Implications for geological CO_2 storage. Advances in Geo-Energy Research, 2025, 15(3): 230-244.
https://doi.org/10.46690/ager.2025.03.06

Abstract:
Subsurface formations typically exhibit heterogeneous wetting characteristics due to the complex pore system, mixed lithology, and prolonged contact with native fluids. This non-uniformity in spatial wettability distribution thus makes the subsurface formations exhibit more complex localized CO_2/brine/rock interactions, introducing uncertainties in estimating trapping capacity and predicting CO_2 plume migration. Field-scale investigation on the role of wettability in CO_2 geo-storage has received limited attention, and previous studies typically assume an internal uniform wettability condition across the whole formation. However, the more realistic scenario of internal wettability spatial variations within a single formation is yet to be thoroughly examined. In this study, a range of experiment-derived wettability-dependent trapping coefficients were utilized to implement the internal wettability heterogeneity in a single formation model, and its impact on CO_2 plume pattern and trapping efficiency was examined. Furthermore, mixed-wet systems with different CO_2-wet fractions were also considered in this study. The results indicate that internal wettability variations result in changes in the local CO_2 saturation pattern and thus impact the overall plume shape and migration. In addition, the internal heterogeneous wettability system exhibits an approximately 35% reduction and an approximately 20% increase in residual trapping capacity in comparison to internal uniform strongly water-wet and uniform weakly water-wet systems, respectively. An increase in the fraction of CO_2-wet regions in the mixed-wet system results in concentrated high-saturation clusters and reduced local CO_2 residual saturation. This further results in reduced residual and dissolution trapping, followed by a linear correlation.

1. Introduction

Consumption of fossil fuels contributes significantly to greenhouse gas (GHG) emissions, which significantly drive climate change and global warming. In particular, as one of the primary GHGs, CO_2 contributes up to 75% of the total GHG emissions (Safi et al., 2023). It is thus necessary to mitigate and control the CO_2 emissions to address the greenhouse effect and achieve the goal of net zero emissions. Underground CO_2 storage has been identified as an effective CO_2 emission reduction option with the potential feasibility of achieving gigatonne-scale storage capacity (Krevor et al., 2023; Wang et al., 2024). This process involves injecting the captured CO_2 into feasible geological formations, such as saline aquifers, unminable coal beds, and depleted oil/gas reservoirs (Wei et al., 2023).

Four significant mechanisms are responsible for CO_2 en-

Yandy Scientific Press

*Corresponding author.
E-mail address: haiyang.zhang@ku.ac.ae (H. Zhang); mmahmoud@kfupm.edu.sa (M. Mahmoud); s.iglauer@ecu.edu.au (S. Iglauer); muhammad.arif@ku.ac.ae (M. Arif).

Received December 11, 2024; revised January 3, 2025; accepted January 24, 2025; available online January 28, 2025.

trapment in subsurface saline aquifers: Structural trapping, residual trapping, dissolution trapping, and mineral trapping. It is recognized that residual and structural trapping mechanisms are more dominant during the early stage of CO_2 storage, while dissolution and mineral trapping can trap CO_2 more safely as the CO_2 either dissolves in brine or forms a solid precipitate. However, these trapping mechanisms are significantly affected by various physicochemical and petrophysical properties of the subsurface formations. In particular, the wettability of the CO_2/brine/rock system, a fundamental physicochemical property, has a crucial influence on CO_2 geostorage regarding the CO_2 plume migration, trapping capacity, and sealing efficiency (Iglauer et al., 2021).

The wetting state of the CO_2/brine/rock systems significantly influences the multiphase fluid flow behaviors (e.g., gas/fluid saturation distribution, relative permeability, flow hysteresis, and capillary pressure) (Arif et al., 2019). Particularly, the brine imbibition process is affected by wettability, resulting in different residual CO_2 saturations under varying wettability conditions. This further impacts the corresponding CO_2 residual trapping capacity at the field-scale. Recent experimental studies have suggested that residual CO_2 saturation in water-wet systems is higher than in mixed-/CO_2-wet systems (Al-Menhali et al., 2016; Rahman et al., 2016). For instance, residual CO_2 saturation reached 8.7% in the oil-wet rock, while it was approximately doubled when the sample had strong water-wetting characteristics (14.9%) (Rahman et al., 2016). This direct influence of wettability on residual entrapment efficiency will also indirectly impact other trapping mechanisms (e.g., dissolution trapping) and thus significantly affect the overall trapping potential of saline aquifers.

While pure and clean mineral surfaces are typically water-wet under subsurface conditions, still the presence of a minute concentration of organic acids can render the subsurface systems CO_2-wet (Ali et al., 2021). Also, prolonged exposure to CO_2 has been shown to tailor the behavior of rock surfaces toward less water-wet (Wang and Tokunaga, 2015). Typically, wettability is characterized via contact angle measurements in the laboratory. In the core-scale experimental measurement, the wettability is often considered uniformly distributed in the core sample, quantitatively represented by a single contact angle. However, a growing body of recent evidence has revealed wettability as a non-uniform and multiscale property (Blunt et al., 2019; Al-Naimi et al., 2023). For instance, carbonate rocks tend to be preferentially oil-wet to intermediate-wet at the macro-scale, while exhibiting a weakly water-wetting state at the micro-scale (Al-Naimi et al., 2023). In addition, a distribution of contact angle is expected as a result of the heterogeneous nature of the grain surface within the rock samples. Andrew et al. (2014) investigated the pore-scale contact angles under reservoir conditions using the micro-CT imaging technique. Results showed a contact angle distribution between 35° to 55°, with an average value of 45°. This variation in contact angles can be attributed to multiple factors, including hysteresis between advancing and receding angles, advancing angle relaxation towards equilibrium, and measurement uncertainty (Andrew et al., 2014). Furthermore, a normal distribution of contact angle within pore space has also been confirmed by different studies (Khishvand et al., 2016; Lv et al., 2017). These experimental observations emphasize the presence of localized variations in contact angles (i.e., internal wettability heterogeneity), despite the overall wettability of the rock sample leaning towards water-wet behavior.

Notably, the internal wettability variations within the formation would be more significant at the field scale. Recent studies revealed that the wetting characteristic of the CO_2/brine/rock system is a function of formation pressure, temperature, salinity, rock roughness, rock mineralogy, and rock surface contaminants (Arif et al., 2019, 2024). Due to the inherent heterogeneity of the subsurface formations, some of these properties are not guaranteed to be uniformly distributed across it. For example, a formation is typically composed of various minerals and roughness patches distributed non-uniformly, which will result in wettability variation in different locations. Therefore, a more complicated localized wettability distribution is expected at the field scale, which will influence the local brine imbibition process and the associated residual trapping capacity in geological CO_2 storage.

Field-scale investigations of the effect of the wetting state on the performance of geological CO_2 storage have received limited attention. The field-scale investigations generally require macroscopic properties, such as hysteresis, relative permeability, and capillary pressure, as inputs to represent the role of wettability. Therefore, different relative permeability curves for various wetting cases have been used to investigate the impact of wettability on the trapping capacity (Al-Khdheeawi et al., 2017; Zhang et al., 2023). Al-Khdheeawi et al. (2018) further applied five distinct relative permeability (drainage and imbibition) and capillary pressure curves derived from rule-of-thumb within a single model with a fixed ratio to represent the wettability heterogeneity. Compared with the homogeneous intermediate-wet case, residual trapping capacity is expected to decrease under heterogeneous wettability conditions (Al-Khdheeawi et al., 2018). However, their approach of assigning drainage and imbibition relative permeability curves may not be rigorous in accurately modeling hysteresis effects, which are essential for the determination of local residual CO_2 saturation. Overall, current studies generally assume a single internal wetting state across the reservoir and thus do not consider the nature of local wettability variations within the formation. This fails to capture the local brine imbibition variations and thus results in overestimations/underestimations of the trapping capacity and uncertainties in predicting plume migration.

Thus, we numerically investigate the impact of internal wettability variations on field-scale geological CO_2 storage in this study. To this end, different scenarios were designed to consider both internal uniform and heterogeneous wettability distribution across the formation. Accordingly, the plume migration dynamics and storage capacity of residual, structural, and dissolution trapping were analyzed. In addition, mixed-wet systems with different fractions of CO_2-wet regions were designed, and the corresponding effects on the effectiveness of CO_2 geo-sequestration were also investigated. The results of this study consider a more realistic wettability characteristic of subsurface formation and thus provide new insights to de-risk

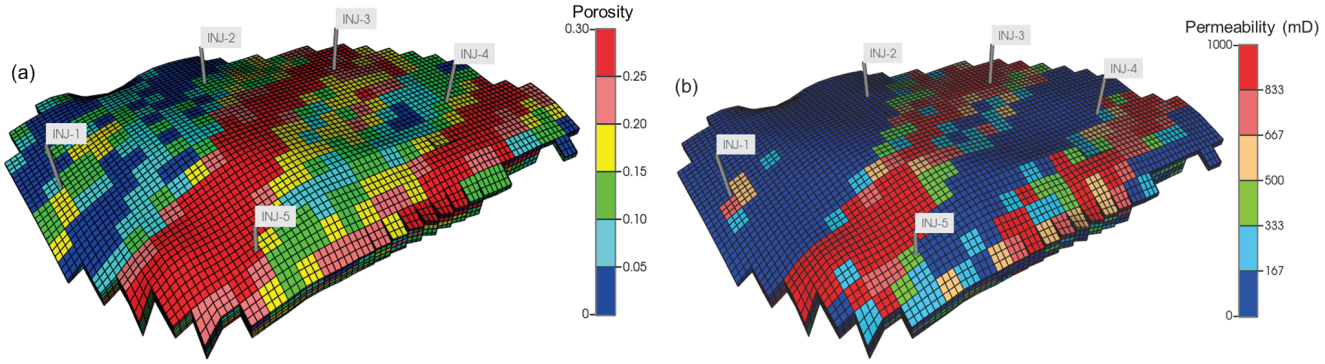

Fig. 1. Spatial distribution of (a) porosity and (b) permeability with the locations of wells.

CO_2 storage under subsurface conditions.

2. Methodology

2.1 Aquifer model

The PUNQ-S3 realistic geologic formation model was used to evaluate the impact of wettability heterogeneity on CO_2 trapping and plume migration in an aquifer setting. This model was developed based on a real field case and has been extensively applied in subsurface studies, including underground H_2/CO_2 storage and enhanced oil recovery. A detailed description of the model can be found elsewhere (Floris et al., 2001; Juanes et al., 2006). The original formation comprises $19 \times 28 \times 5$ blocks, of which 1,761 blocks were actively involved in the simulation. Each grid cell is characterized by dimensions of 180 m along both the x and y axes and approximately 3 m in the z direction. The PUNQ-S3 model was artificially tailored to include variations in terms of grid refinement, formation depth, well locations, well operations, fluid properties, and relative permeability curves. For example, each grid cell is refined into $3 \times 3 \times 1$ grid blocks to enhance precision in evaluating CO_2/brine flow dynamics and associated trapping estimations.

The formation top is located at a depth of 1 km with an initial pressure of 10 MPa. The system is considered isothermal with a constant temperature of 343 K. We set the aquifer salinity at 10 wt% NaCl. The corresponding brine and CO_2 properties under the prevailing reservoir conditions were modeled using CMG-WinProp^{TM} module. The average porosity is 20%, while the permeability in horizontal directions measures 100 mD, with a vertical-to-horizontal anisotropy ratio of approximately 0.5. The corresponding spatial distributions are presented in Fig. 1. The lateral boundary blocks are assigned a significantly larger pore volume to represent an infinite aquifer (Juanes et al., 2006; Zhang et al., 2025), allowing native brine to leave the system once CO_2 is injected. In addition, the top and bottom boundaries are set as no-flow conditions, preventing CO_2 leakage beyond the model domain. It should be noted that a fully closed system would result in a significant pressure increase once CO_2 is injected. This pressure buildup would increase the density of the injected CO_2, thereby reducing its specific volume under reservoir conditions. Consequently, the same injected volume at the surface would occupy a smaller reservoir volume, leading to a reduced spatial extent of the CO_2 plume. Additionally, higher pressure enhances CO_2 solubility in brine, potentially enhancing dissolution trapping. However, it is important to note that dissolution trapping also depends on the CO_2-brine contact area (e.g., plume extent), which may be reduced under high-pressure conditions.

2.2 Wettability heterogeneity implementation

It has been consistently reported that wettability strongly influences the residual CO_2 saturation while exhibiting limited impact on the initial CO_2 saturation (Al-Menhali et al., 2016; Rahman et al., 2016; Basirat et al., 2017). The relationship between the residual CO_2 saturation and the initial CO_2 saturation is typically described by the initial-residual (IR) curve, which can also be used to illustrate the CO_2 trapping behaviors within the pore space. We thus reviewed and collected the experimental data pairs of CO_2 saturations at initial and residual states in two distinct wettability scenarios (i.e., water-wetting and CO_2-wetting) from literature, as shown in Fig. 2. Detailed information can be found in our previous study (Zhang and Arif, 2024). It is important to note that the existing research primarily focuses on water-wet conditions, with limited investigations addressing comparisons between various wettability systems. The IR curves are determined using the Land trapping model, represented as follows:

$$C = \frac{1}{S_{CO2,r}} - \frac{1}{S_{CO2,i}} \tag{1}$$

where C is the trapping coefficient, $S_{CO2,r}$ is the residual CO_2 saturation, and $S_{CO2,i}$ is the initial CO_2 saturation. The obtained C value can then be employed to generate the imbibition relative permeability curves for field-scale simulations.

Clearly, the water-wet data pairs fail to converge on a single trapping coefficient; instead, they lie between two C bounds (Fig. 2). These variations of data points are attributed to variability in fluid properties and operating conditions in respective studies, which is consistent with previous observations (Krevor et al., 2015; Alyafei and Blunt, 2016). According to Krevor et al. (2015), the IR trapping of a given CO_2/brine/rock system remains invariant under varying temperature, brine salinity, and pressure, as long as the wettability characteristics are comparable across different systems. This means the impact

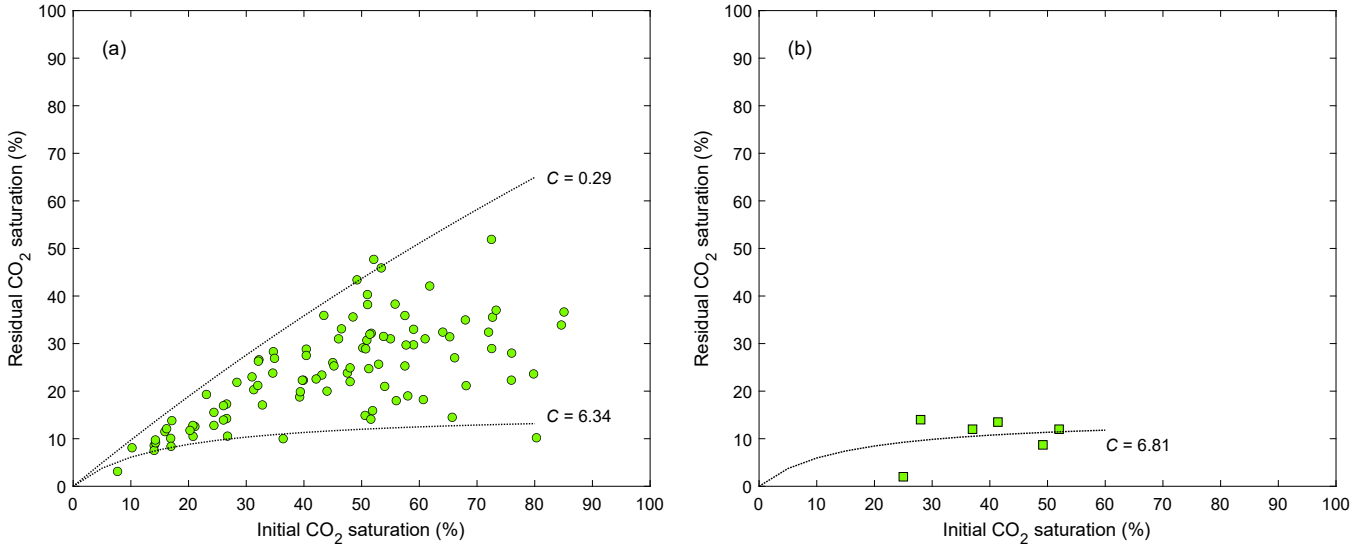

Fig. 2. IR trapping curves for the system with (a) water-wetting characteristics and (b) CO_2-wetting characteristics, modified after Zhang and Arif (2024).

of those influencing factors on the IR trapping curve depends on their ability to influence the CO_2/brine/rock wettability. Therefore, the variations in the trapping coefficient (C values) can indicate wettability heterogeneity despite all the data points exhibiting an overall water-wet characteristic. However, CO_2-wet data pairs, despite being limited, tend to collapse in one curve (Fig. 2), suggesting a more straightforward and universally applicable pattern of residual trapping behaviors in CO_2-wet systems.

It is claimed that the trapping coefficient values (or IR curves) are significantly controlled by the wettability characteristics of the CO_2/brine/rock system (Alyafei and Blunt, 2016; Øren et al., 2019). Therefore, in this study, experimentally derived trapping coefficients were utilized to model the wettability-dependent hysteresis effects at various locations within a single formation, thereby representing the internal spatial wettability variations. This approach enables more accurate modeling of the local hysteresis process by accounting for spatial variations in wetting characteristics. We considered the internal wettability heterogeneity in an overall water-wet formation, which means the experimentally derived trapping coefficients were all collected from the water-wet conditions. In addition, a mixed-wet formation, which includes heterogeneous water-wet and uniform CO_2-wet characteristics, is also considered in this study. Although wettability heterogeneity can also be employed to describe the coexistence of both water-wetting and CO_2-wetting regions within the formation, for clarity and differentiation, we refer to these conditions as a mixed-wet system in this study. The wettability heterogeneity is only used to represent the internal non-uniform wettability characteristic in an overall water-wet formation.

Based on the above analysis and discussion, the trapping coefficient (C values) can be used as a suitable metric for characterizing the influence of wettability on residual trapping behavior. Therefore, a singular C value will be utilized in simulations to depict a distinctive wetting state, thereby facilitating the implementation of internal heterogeneous wettability systems by assigning different C values to different gridblocks. It is important to highlight again that the range of trapping coefficients (i.e., 0.29-6.34 for water-wet state and 6.81 for CO_2-wet state) used in this study is adopted from our previous review (Zhang and Arif, 2024), which systematically summarized experimental trapping data from various studies, where CO_2 remained in the supercritical state, consistent with the designed PUNQ-S3 reservoir conditions (i.e., 10 MPa and 343 K). These trapping coefficients are also applicable to both sandstone and carbonate reservoirs. In addition, the PUNQ-S3 model is a well-known synthetic benchmark model in field-scale reservoir simulations. Thus, its geological structure and well-documented properties make it a useful reference for assessing the impact of wettability on CO_2 geological storage. Overall, the selected trapping coefficients and geological model can provide a basis for future replication and comparative analyses.

The drainage relative permeability in an overall water-wet system is assumed to be consistent across the formation (Fig. 3(a)), while the distinct imbibition relative permeability curves were utilized for each gridblock due to the internal wettability variations (i.e., varying C trapping coefficients, Fig. 2). The imbibition relative permeability is molded by the C trapping coefficient, which is given by:

$$K^I_{r\mathrm{CO_2}}\left(S_{\mathrm{CO_2}}\right) = K^D_{r\mathrm{CO_2}}\left[\frac{S_{\mathrm{CO_2}} - S_{\mathrm{CO_2},r}}{S_{\mathrm{CO_2},i} - S_{\mathrm{CO_2},r}} S_{\mathrm{CO_2},i}\right] \tag{2}$$

where $K^I_{r\mathrm{CO_2}}$ is the CO_2 imbibition relative permeability; $K^D_{r\mathrm{CO_2}}$ is the CO_2 drainage relative permeability (Fig. 3(a)); $S_{\mathrm{CO_2}}$ is the CO_2 saturation; $S_{\mathrm{CO_2},r}$ is the residual CO_2 saturation than can be determined through Eq.(1) with a known C value. The generated imbibition relative permeability curves for the CO_2

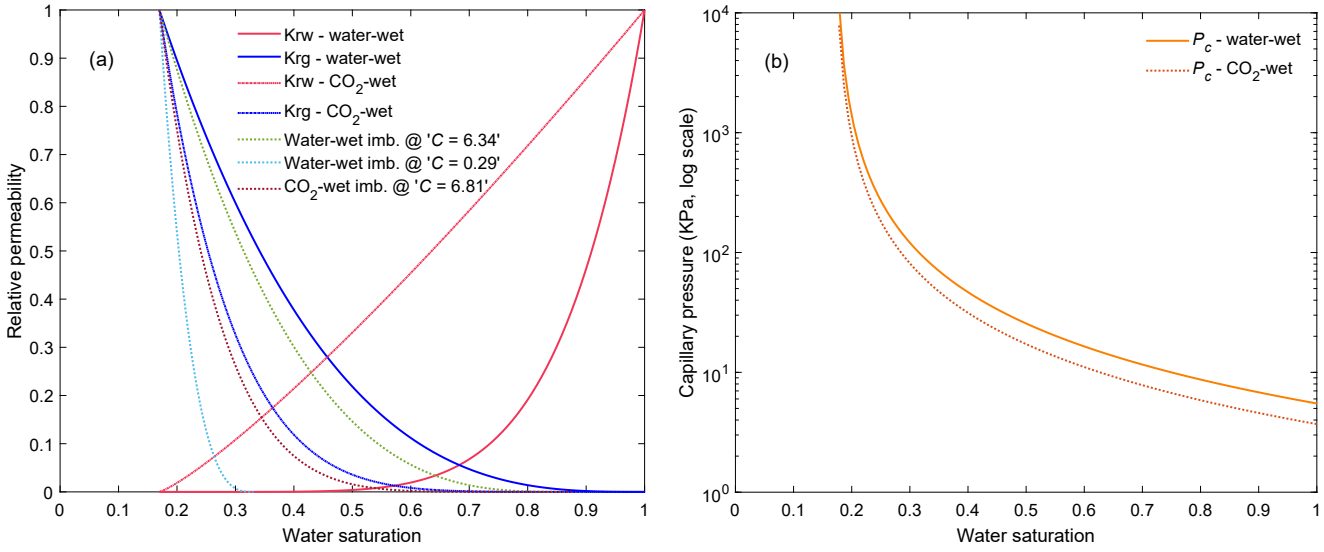

Fig. 3. (a) Drainage CO_2-bine relative permeability curves with the generated imbibition relative permeability curves based on different trapping coefficients and (b) capillary pressure curves for different wetting systems.

phase with different wettability-dependent C values are illustrated in Fig. 3(a). It is also important to note that the impact of wettability on the drainage relative permeability in an overall water-wet system is not considered in this study as there are quite limited experimental studies focusing on this subject (Arjomand et al., 2020; Chang et al., 2020; Hu et al., 2017). The current literature lacks solid evidence to effectively model the drainage relative permeability under variable water-wet conditions within the CO_2/brine/rock systems. However, this study employed different relative permeability and capillary curves for the water-wet and CO_2-wet systems (Fig. 3). The water-wet curves are adopted from (Niu et al., 2015) while the CO_2-wet curves are selected from (Bachu, 2013). Although those experimental conditions do not strictly match our geological model setup, their main characteristics remain applicable to the objectives of this study. Specifically, the relative permeability data from (Niu et al., 2015) represent a water-wet system, while the data from (Bachu, 2013) indicate a CO_2-wet system, providing an effective approach to account for wettability variations in our analysis. It is also important to note that there is currently a lack of experimental studies that simultaneously measure both relative permeability and capillary pressure under different wettability conditions within the same system. Thus, this selection allows us to systematically investigate the impact of wettability variations on CO_2 trapping and plume migration, which is a key objective of this study.

2.3 Simulation setup

Five injection wells were perforated to facilitate the CO_2 injection (Fig. 1), each with a surface injection rate of 8,000 m^3/day. This results in a total injected volume of approximately 0.25 pore volume of the aquifer, allowing a comprehensive analysis of all three trapping mechanisms (i.e., dissolution trapping, residual trapping, and structural trapping). The injection period lasts for 10 years, followed by a 190-year storage period. Different simulation scenarios were designed to assess the influence of heterogeneous wettability on the performance of CO_2 geo-sequestration, as outlined in Table 1.

All the simulation cases were grouped into three groups, namely water-wetting, CO_2-wetting, and mixed-wetting. Within the water-wet simulation group, two distinct scenarios were examined. One scenario exclusively considered residual trapping, while the other incorporated both residual trapping and dissolution trapping. Given the relatively short storage simulation timescale (190 years) and slow reaction rate between fluid and rock, the contribution of mineral trapping is minimal and therefore neglected in this study. Furthermore, each scenario includes the same set of simulation cases, including two single uniform wettability cases with different single trapping coefficients and two internal heterogeneous wettability cases. Both random and normal distributions of wettability were considered in the internal wettability heterogeneity cases, and the corresponding histograms of trapping coefficient values used in the simulation are presented in Fig. 4. Note that three realizations of random selection for water-wet trapping coefficients were undertaken, given the uncertainties and inherent randomness in the selection process. It is also important to highlight that while internal wettability variations within the formation were considered in this study, the system as a whole still maintains an overall water-wet characteristic (i.e., the C values are constrained within two specified bounds).

The random and normal wettability distributions are assumptions rather than representations derived from actual reservoir characterization. However, the random wettability distribution is helpful particularly when formation data are sparse in the early stages of field development. It can effectively represent high wettability variation in different regions.

Table 1. Simulation scenarios considered in this study.

Group	Simulation scenarios	Wettability (C value)	Residual trapping	Dissolution trapping
Water-wet	1	Uniform strongly water-wet ($C = 0.29$)	Yes	No
		Uniform strongly water-wet ($C = 6.34$)	Yes	No
	2	Random wettability distribution ($C = 0.29 - 6.34$)	Yes	Yes
		Normal wettability distribution ($\mu = 3.315$, $\sigma = 0.08$)	Yes	Yes
CO_2-wet	3	CO_2-wet ($C = 6.81$)	Yes	Yes
Mixed-wet	4	CO_2-wet fraction = 0.25	Yes	Yes
	5	CO_2-wet fraction = 0.5	Yes	Yes
	6	CO_2-wet fraction = 0.75	Yes	Yes

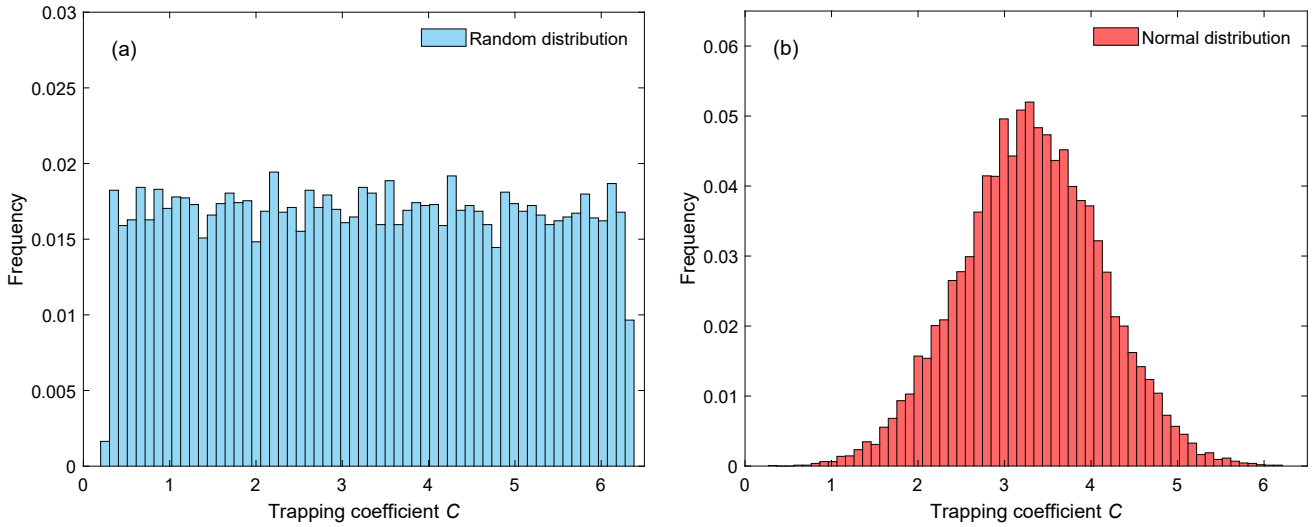

Fig. 4. Trapping coefficient used in the simulation with (a) a random distribution and (b) a normal distribution.

Similarly, the normal wettability distribution can be used to represent gradual wettability trends, which can be induced by diagenetic or depositional effects. This is supported by the fact that normal or log-normal distributions of contact angles are commonly observed in pore-scale studies (Andrew et al., 2014; Lv et al., 2017). Thus, from a realistic perspective, a normal wettability distribution may better reflect reservoir-scale wettability variations. In contrast, a random distribution is more sensitive to local pore-scale heterogeneities because it assumes no spatial correlation between trapping coefficients in adjacent gridblocks, leading to highly localized variations in the CO_2 distribution. The choice of wettability distribution should consider geological settings and data availability. If detailed core-scale wettability and mineralogy data are available, a site-specific distribution is preferable. Otherwise, a normal distribution is suitable for relatively homogeneous formations, while a random distribution may better capture highly heterogeneous or fractured reservoirs. Additionally, sensitivity analyses using both distributions can help quantify uncertainties and improve CO_2 trapping and migration predictions.

Mixed-wet systems with different CO_2-wet fractions (i.e., 0.25, 0.5, and 0.75) were systematically examined, as detailed in Table 1 (mixed-wet group). This is implemented by randomly allocating a specific fraction of gridblocks with a CO_2-wet trapping coefficient ($C = 6.81$) and the CO_2-wet relative permeability and capillary pressure curves, while the remaining grid cells were assigned water-wet characteristics (i.e., trapping coefficients ranging randomly from 0.29 to 6.34, water-wet relative permeability, and water-wet capillary pressure curve). This approach provides a simplified yet controlled way of investigating the impact of mixed-wetting characteristics on CO_2 trapping.

3. Results and discussion

3.1 Impact of internal wettability heterogeneity on plume migration

The influence of internal heterogeneous wettability distribution on the migration of CO_2 plume was examined based

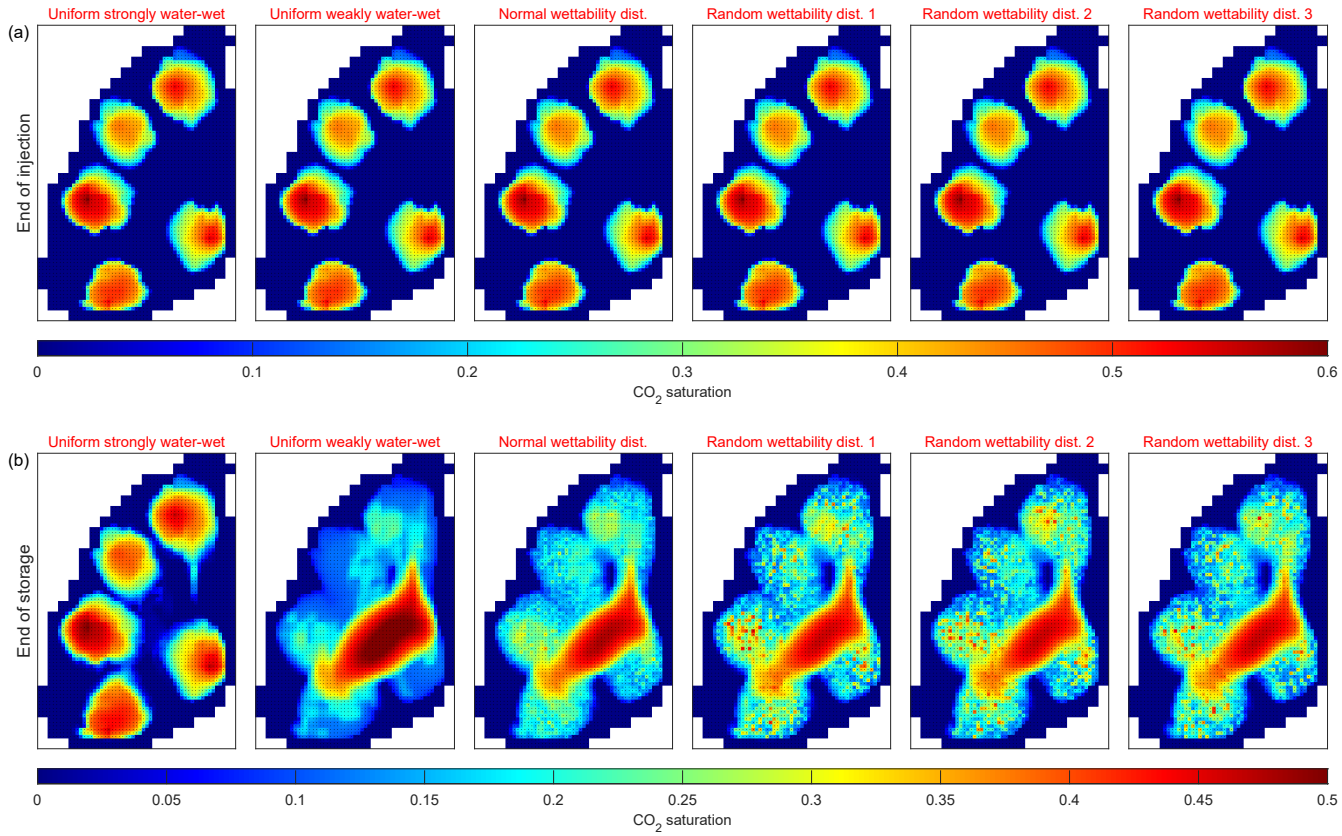

Fig. 5. CO_2 saturation distribution at the top layer under different wettability cases at the end of (a) injection and (b) storage. Note that the legend scales are different between the two figures (0-0.6 for (a) and 0-0.5 for (b)) to enhance the contrast between different wettability cases.

on the results without considering the dissolution trapping mechanism. The CO_2 plume dynamics at the top layer of different cases are presented in Fig. 5. Upon CO_2 injection, the CO_2 migrates upwards, driven by the buoyant force. In addition, the geologic features, i.e., a dome at the center of the aquifer model, also facilitate migration towards the formation's top center. During the injection of CO_2, the CO_2 is displacing brine in a drainage-like process. Since the impact of wettability on the drainage process is not considered, the CO_2 saturation distribution is comparable in all cases (Fig. 5(a)). However, the imbibition process occurs during the subsequent CO_2 storage period, which is strongly influenced by wettability as reported by previous observations (Al-Menhali et al., 2016; Zhang et al., 2023). Therefore, different plume migration patterns are observed under different wettability conditions (Fig. 5(b)). For instance, the plume movement toward the central dome was impeded in the uniform strongly water-wet system ($C = 0.29$) with a lower single trapping coefficient, resulting in less accumulated mobile CO_2 in the formation's top center. Conversely, the uniform weakly water-wet system ($C = 6.34$) exhibits a larger CO_2-enriched accumulation area (Fig. 5(b)). These observations indicate that the CO_2 plume experiences a longer migration distance in the less water-wet system, which agrees with the findings in previous studies (Al-Khdheeawi et al., 2017, 2018; Zhang et al., 2023).

However, when the internal wettability variations are considered, more compact and constrained CO_2 accumulation areas are observed compared with the uniform weakly water-wet system. Additionally, the overall plume shape and migration dynamics in different internal wettability heterogeneity cases were comparable. However, the internal wettability heterogeneity results in variations in the local CO_2 saturation, which is attributed to the different local imbibition processes. Two additional observation points along the migration path, i.e., gridblock #(47, 25, 1) and gridblock #(24, 71, 1), were selected to investigate the local CO_2 saturation variations (Fig. 6). The CO_2 saturation of each gridblock initially increases to the maximum value (around 0.40 in Fig. 6(a) and around 0.45 in Fig. 6(b)) during the injection period, followed by a decrease to the residual value after the imbibition. The extent of this reduction is thus a strong function of the wettability. The results indicate that the uniform strongly water-wet system exhibited a lower maximum CO_2 saturation in observation point #(47, 25, 1), which is mainly attributed to the reduced volume of CO_2 reaching this grid cell to achieve the residual water saturation state. In addition, the uniform strongly water-wet system also undergoes an earlier reduction in CO_2 saturation in both observation points. This is also explained by the lower volume of CO_2 consistently filling in the observation points, resulting from an increased trapped amount of CO_2 by previously invaded grid cells. Consequently, an earlier imbibition process occurs at the observation points.

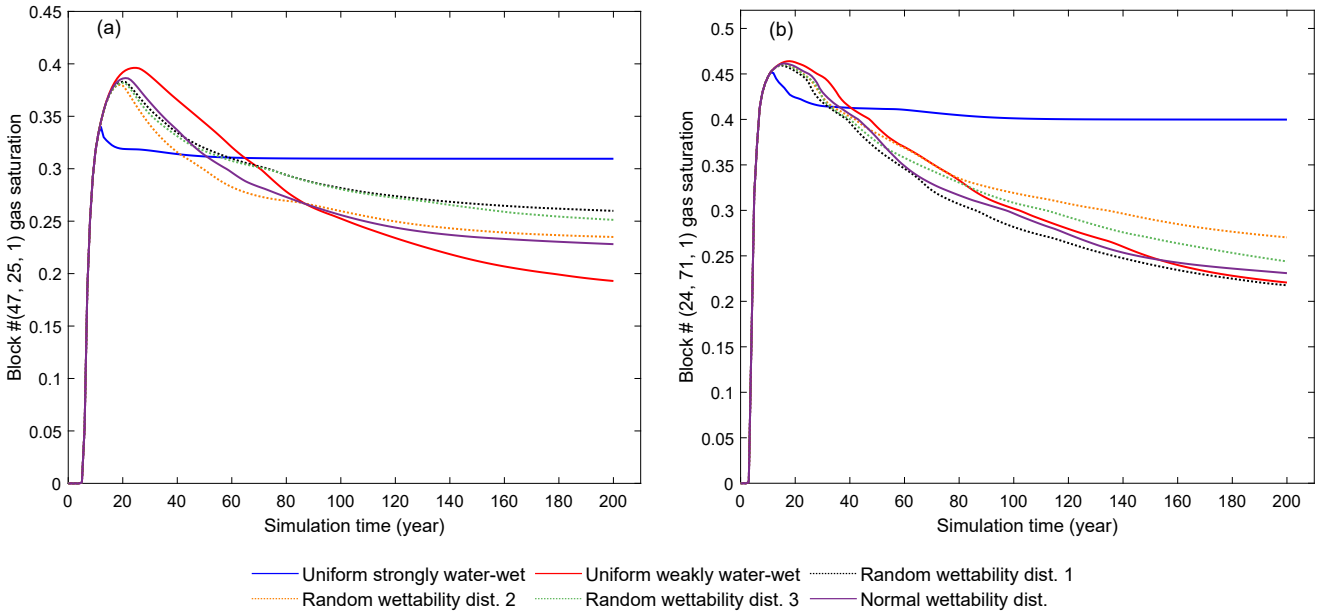

Fig. 6. Local CO_2 saturation dynamics in two observation points of (a) block #(47, 25, 1) and (b) block #(24, 71, 1).

It is also clear that the internal wettability variations result in different residual CO_2 saturations in different locations (Fig. 6), yet these values remain within the range observed under two uniform wettability conditions. These phenomena are caused by the variations of local trapping coefficients in different internal wettability heterogeneity implementations. Therefore, it is concluded that the internal wettability heterogeneity strongly influences plume migration dynamics in the storage phase and the corresponding local CO_2 saturation history.

Comparing the CO_2 saturation distribution between the normal and random wettability distribution cases (Fig. 5(b)), it is evident that the normal wettability distribution leads to a more concentrated high-saturation region, particularly at the central dome. In contrast, the random wettability distribution leads to more extensive localized high-saturation zones along the migration path. This difference is because the normal distribution exhibits a relatively greater continuity in the wettability, making CO_2 more likely to accumulate in the central dome, while random wettability variations create a more dispersed migration pathway. This also indicates that the normal wettability distribution tends to exhibit an overall longer CO_2 migration path. However, the local wettability randomness may still create dominant pathways that allow CO_2 to possibly travel even farther. This is supported by Fig. 6, where a shorter time is observed for the observation point to reach maximum CO_2 saturation, indicating faster migration along preferential pathways. Further investigation is needed to assess this behavior under different geological structures and injection strategies.

3.2 Impact of internal wettability variations on residual trapping

The influence of internal wettability heterogeneity on residual entrapment capacity was examined by comparing the trapping amount of different internal heterogeneous wettability cases with the two uniform wettability cases without considering CO_2 solubility. The corresponding residually trapped CO_2 is presented in Fig. 7(a). For instance, the quantities of the residual trapped CO_2 are 1.64×10^5 tons (60.13%), 1.55×10^5 tons (56.83%), 2.57×10^5 tons (94.11%), and 1.02×10^5 tons (37.42%) for the random wettability distribution system (1^{st} random realization), normal wettability distribution system, uniform strongly water-wet system, and uniform weakly water-wet system, respectively. Note that these values are obtained from the software output and subsequently converted to the desired units. Clearly, the residual trapping capacities of systems exhibiting internal wettability variations fall within the range defined by the trapping capacities of the two uniform wettability systems. Notably, the internal heterogeneous wettability system demonstrates an approximately 35% reduction in residual trapping capacity when compared with the uniform strongly water-wet system while exhibiting an approximately 20% enhancement in comparison to the uniform weakly water-wet system. These observations indicate that the estimation of residual trapping potential based on single wetting characteristics of the formation will lead to underestimations or overestimations, thereby introducing uncertainty in the CO_2 geo-storage capacity estimations.

Note that the residual trapping amount in different random wettability distribution cases is notably comparable, with 1.64×10^5 tons for the 1^{st} realization, 1.65×10^5 tons for the 2^{nd} realization, and 1.64×10^5 tons for the 3^{rd} realization, respectively (Fig. 7(a)). This observation suggests that different random assignments of trapping coefficient into each gridblock

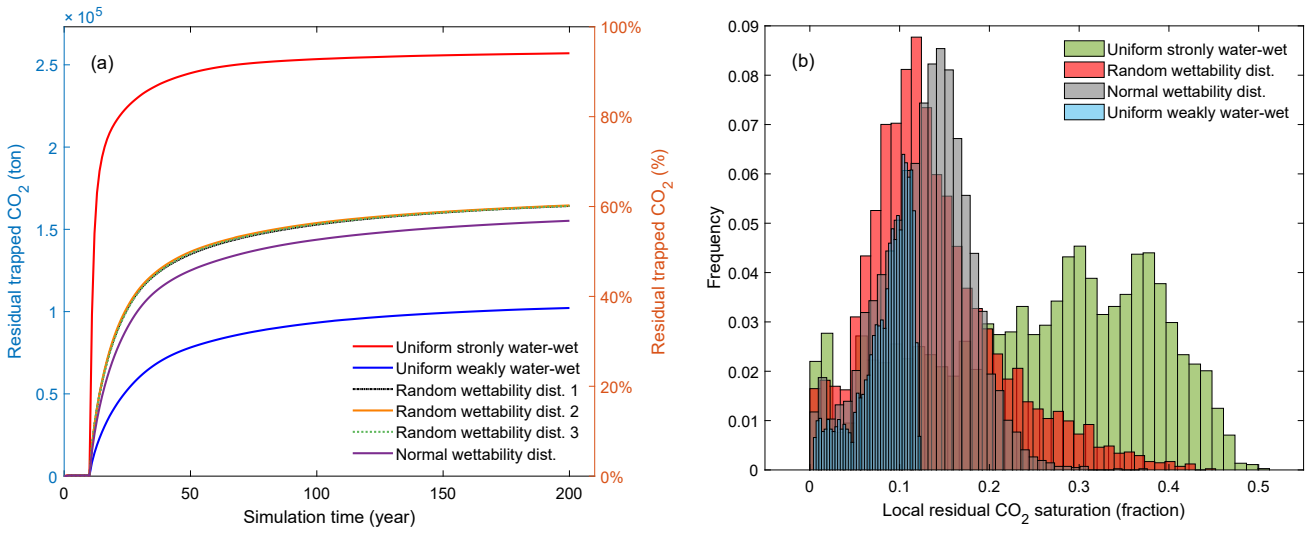

Fig. 7. (a) Residual CO_2 trapping capacity in different wettability cases and (b) the corresponding local residual CO_2 saturation distribution.

do not strongly influence the residual trapping capacity. The calculation of residual trapping capacity is a function of local residual CO_2 saturation, gridblock volume, and the number of gridblock (Ershadnia et al., 2023), which can be expressed by:

$$M_t = \sum_{n=1}^{N} \rho_n \times \phi_n \times V_n \times S_{gr,n} \tag{3}$$

where M_t is the total capacity of tapped CO_2, S_{gr} is the local residual CO_2 saturation, ρ is the CO_2 density, V is the gridblock pore volume, N is the total number of grid cells, and ϕ is the porosity. Therefore, despite variations in residual CO_2 saturation across individual grid cells, the substantial number of gridblocks resulting from grid refinement and the large CO_2-occupied volume mitigates the impact of local saturation variations. This is further validated through an examination of the effect of gird resolution on the trapping efficiency in systems with random wettability distribution, as detailed in Supplementary Information. Specifically, in a coarse-grid (low-resolution) model, each grid cell covers a larger spatial domain, while the total number of grid cells is limited. As a result, the wettability of a single gridblock has a more significant impact on the overall trapping. Since the wettability is assigned randomly, different random realizations may lead to significantly different local wettability distributions, which in turn leads to strong fluctuations in trapping estimation among different realizations. In other words, coarse grid blocks amplify the effect of local wettability randomness, as the contribution of a single grid block becomes more significant, resulting in higher variations in residual trapping. In contrast, with finer gridblocks, random wettability assignments are distributed across a larger number of cells, reducing the influence of individual gridblock wettability on the overall trapping. This minimizes differences between different random realizations, leading to more stable trapping estimates.

The distributions of local residual CO_2 saturation in different cases are presented in Figs. 7(b) and 8. In the uniform strongly water-wet system ($C = 0.29$), a greater portion of residual CO_2 saturation is observed within the range of 0.2 to 0.5 than in other cases. Conversely, in the uniform weakly water-wet system, the residual CO_2 saturation is predominantly below the threshold of approximately 0.1. These findings are consistent with the previous experimental measurements that suggest a higher residual CO_2 saturation in more water-wet systems (Al-Menhali et al., 2016; Rahman et al., 2016). In addition, the random wettability distribution system shows a relatively broad distribution of residual CO_2 saturation, with a noticeable peak within a specific range but extending across a wide spectrum of saturation levels, whereas the normal wettability system displays a narrower, more localized distribution of residual saturation following a normal pattern. The spatial distribution of residual CO_2 saturation (Fig. 8) also indicates that the internal wettability variations will result in more pronounced variations in the local CO_2 saturation distribution. Specifically, residual CO_2 saturation under the normal wettability distribution exhibits a relatively smoother spatial variation (Fig. 8), whereas the random distribution cases show pronounced fluctuations. This difference is quantitatively confirmed by the calculated variance of residual CO_2 saturation, which is 0.003296 for the normal distribution case and 0.006779 for the random distribution case in Fig. 8, showing a nearly double increase in variance. The higher variance in the random wettability distribution indicates a more heterogeneous local residual CO_2 distribution, indicating that trapping efficiency varies unevenly across the domain.

3.3 Impact of internal wettability heterogeneity on overall trapping capacity

In this section, the interaction between dissolution and residual trapping is considered to examine the influence of wettability variations on total trapping capacity (i.e., dissolution, structural, and residual trapping). The CO_2 plume migration patterns for different cases are presented in Fig.

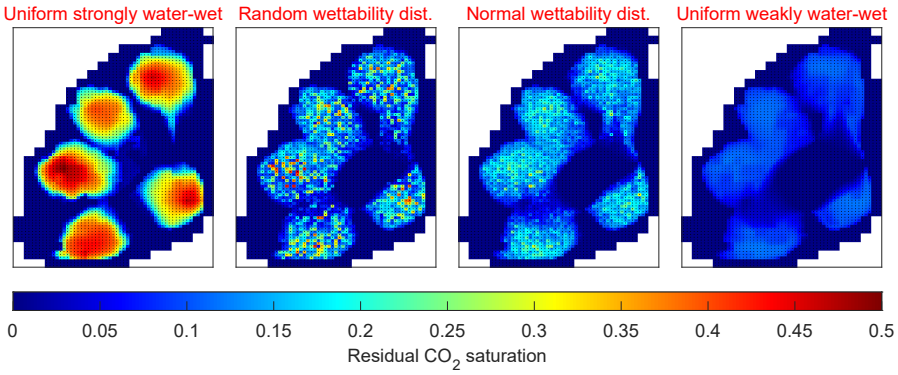

Fig. 8. Residual CO_2 saturation distribution at the top layer of different wettability scenarios.

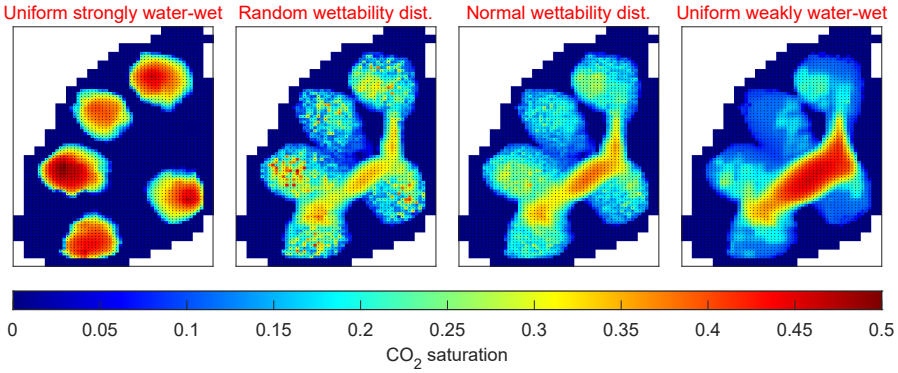

Fig. 9. CO_2 saturation distribution at the top layer of different wettability scenarios considering both residual and dissolution trapping mechanisms.

9. Apparently, the uniform water-wet system shows highly localized regions of high CO_2 saturation, while the random wettability distribution displays a more dispersed saturation pattern, covering a wide range of low to medium saturation levels. In the central regions, however, the normal wettability distribution exhibits more concentrated saturation compared to the random case. Moreover, compared to the case with residual trapping only (Fig. 5(b)), the inclusion of the CO_2 solubility results in a lower overall CO_2 saturation and fewer localized high-saturation areas. This is attributed to CO_2 consumption during the migration process, where dissolution in fresh brine gradually reduces the free CO_2 saturation in the system.

The residual and dissolution trapping capacities of all considered cases are presented in Fig. 10. Residual entrapment capacity followed the similar trend observed in Section 3.2, wherein the residual trapping capacity of an internal heterogeneous wettability system lies between the values of two uniform wettability systems (Fig. 10(a)). In terms of dissolution trapping, all the cases exhibit similar trapping performance during the CO_2 injection period (i.e., the first 10 years in Fig. 10(b)). Note that dissolution trapping largely depends on CO_2 solubility and the contacting area between brine and CO_2. The similarity in CO_2 plume spread-out during the injection period, as illustrated in Fig. 5(a), consequently leads to comparable dissolution trapping capacities across different scenarios. It is also important to note that dissolution trapping manifests throughout the entire operational lifespan of the CO_2 geo-storage projects as long as free CO_2 comes into contact with fresh brine (i.e., the brine is not fully saturated with CO_2). Therefore, the dissolution trapping amount increases with the increase in the simulation time (Fig. 10(b)).

The dissolution trapping capacities in the internal heterogeneous wettability systems, including random and normal wettability distribution, exhibit similar values ranging from $1.09 \times 10^5 - 1.11 \times 10^5$ tons, which also falls between the capacities of the other two single wettability systems. However, the uniform strongly water-wet system leads to the lowest dissolution trapping. This phenomenon is primarily attributed to the enhanced residual trapping, which results in a reduced amount of free CO_2 coming into contact with fresh brine, consequently reducing the dissolution trapping capacity. Fig. 11, which supplements Fig. 10, summarizes the trapping inventory for all considered cases. As storage time increases, the amount of residual and dissolution trapping increases, while the amount of mobile CO_2 decreases. In a uniformly strongly water-wet system, nearly all injected CO_2 is trapped by residual and dissolution trapping (see Fig. 10 for exact values), leaving only approximately 0.26% as mobile CO_2. However, in systems with wettability heterogeneity or weakly water-wet conditions, CO_2 is less effectively trapped and tends to migrate toward the central dome (see Fig. 9) and accumulate under the caprock as a mobile phase. Specifically, the percentage of mobile CO_2 is 15.17% for the 1st realization of random wettability distribution, 15.04% for the

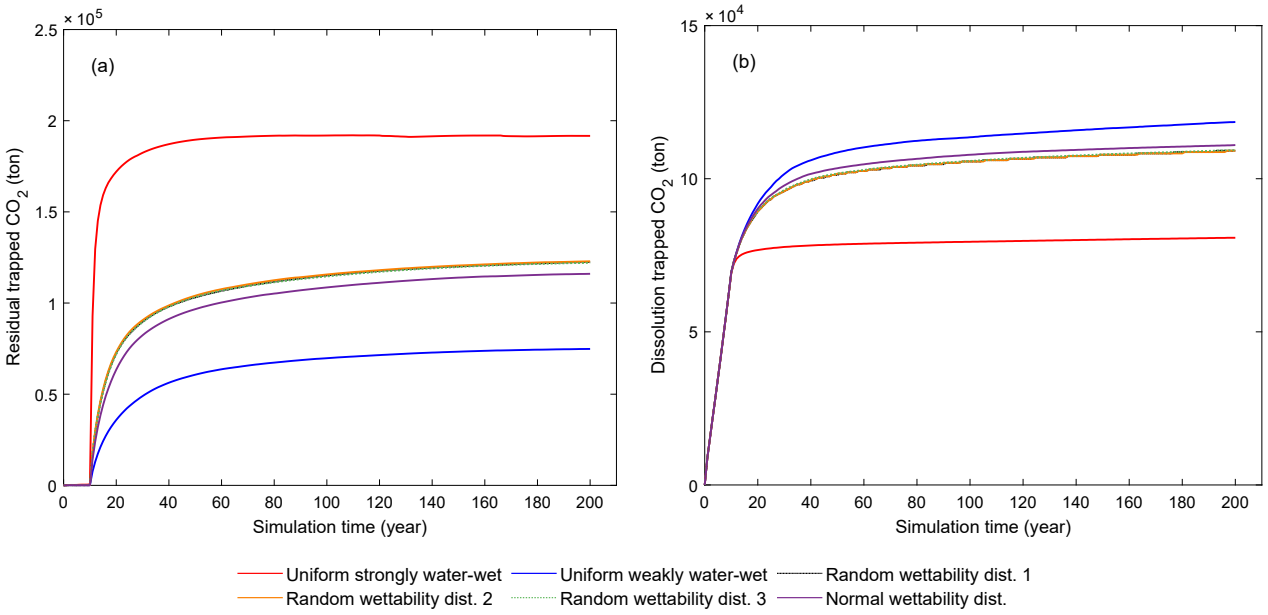

Fig. 10. Trapping capacity of (a) residual entrapment and (b) dissolution.

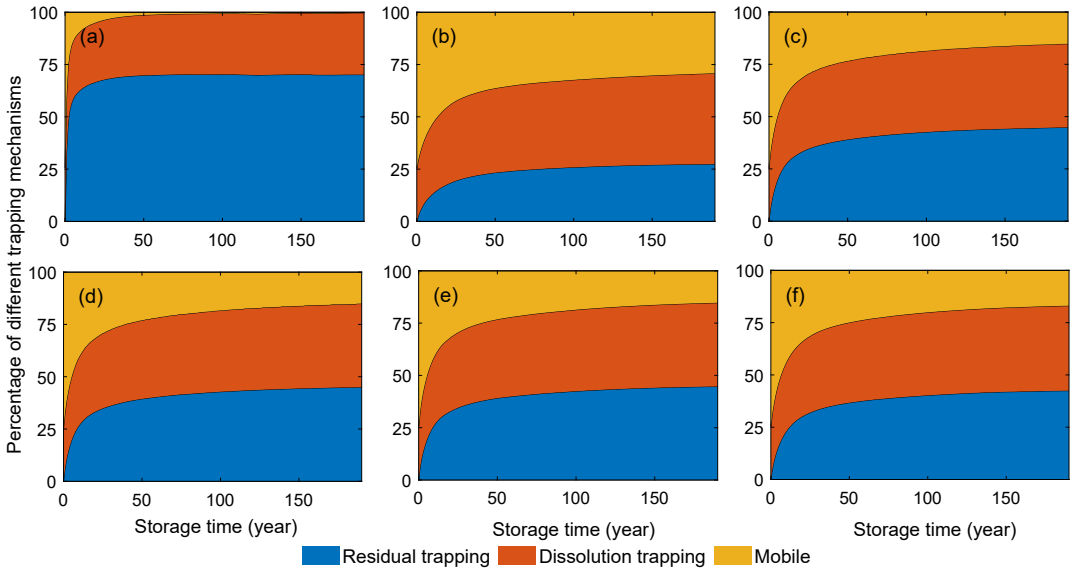

Fig. 11. Trapping inventory of different wettability cases: (a) Uniform strongly water-wetting, (b) uniform weakly water-wetting, (c) random wettability distribution (1st realization), (d) random wettability distribution (2nd realization), (e) random wettability distribution (3rd realization), and (f) normal wettability distribution.

2nd realization of random wettability distribution, 15.25% for the 3rd realization of random wettability distribution, 16.87% for the normal wettability distribution case, and 29.21% for the weakly water-wet case. It is, therefore, concluded that the residual and dissolution trapping capacities of internal wettability heterogeneity cases fall within the range of capacities exhibited by the two single uniform wettability systems. Furthermore, the wettability variation in an overall water-wet system is shown to exert an indirect influence on dissolution trapping by directly affecting residual trapping.

The results also indicate that while the total CO_2 storage capacity is similar between the random and normal wettability distributions (Figs. 10 and 11), the impact of the wettability distribution pattern on local CO_2 saturation is more pronounced (Fig. 9). A random wettability distribution leads to multiple local regions with high saturations, while more CO_2 preferentially accumulates under the central dome for the normal wettability distribution case. From a risk assessment perspective, the first scenario presents a higher likelihood of small-scale mobile CO_2 clusters at various points while the caprock integrity is the primary concern for the second scenario.

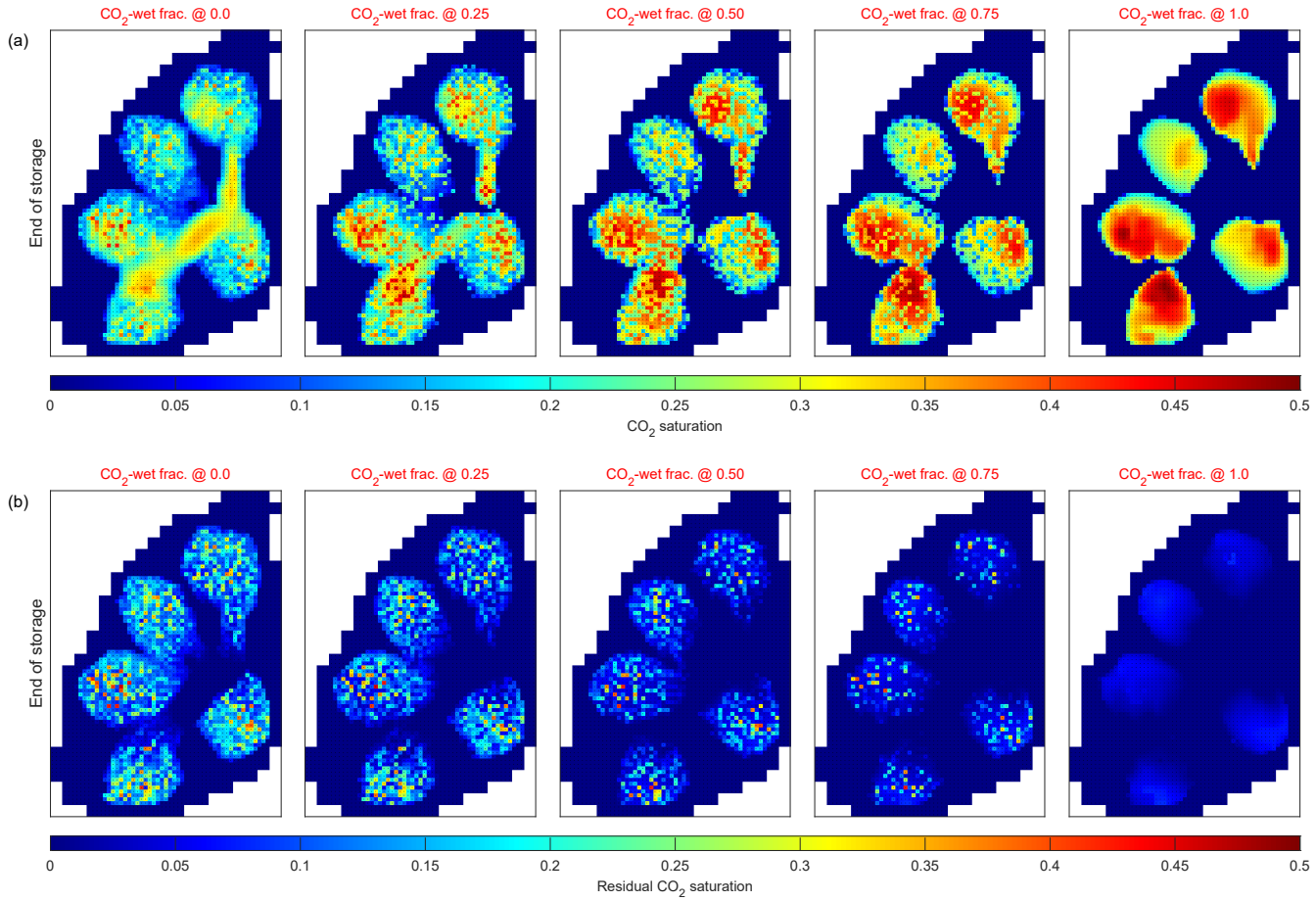

Fig. 12. (a) Plume migration and (b) residual CO_2 saturation distribution at different wet-fraction conditions. Note that the case with a CO_2-wet fraction of 0 is equivalent to the random wettability distribution case (1st realization).

3.4 Impact of mixed-wet condition on CO_2 trapping

In the previous sections, the internal wettability variations in an overall water-wet system were considered. To assess the effects of mixed-wet conditions on CO_2 trapping capacity, different fractions of CO_2-wet regions, including 0, 0.25, 0.5, 0.75, and 1, were considered (see Table 1). The corresponding plume migration and the residual CO_2 saturation distribution are presented in Fig. 12. It is clear that as the CO_2-wet fraction increases from 0.0 to 1.0, the plume distribution shifts from a widespread, low-saturation spread to concentrated high-saturation clusters in specific areas (Fig. 12(a)). This trend occurs because CO_2-wet conditions decrease the relative permeability of the CO_2 phase (see Fig. 3(a)), which reduces its mobility to flow through the pore spaces. Consequently, CO_2 tends to form localized high-saturation clusters, reducing its overall spread across the reservoir. Similarly, as shown in Fig. 12(b), the local residual CO_2 saturation decreases significantly as the CO_2-wet fraction increases, indicating that CO_2 becomes less likely to be trapped.

Residual and dissolution trapping results are illustrated in Fig. 13. The residual trapping capacity is observed to decrease with the increase in the CO_2-wet fraction (Fig. 13(a)). For example, the aquifer with 25% regions being CO_2-wet exhibits a residual trapping potential of 1.0×10^5 tons (36.69%). However, the residual trapping capacity reduces to 7.04 × 104 tons (23.63%) in the scenario where the CO_2-wet regions comprise 75% of the formation (i.e., a reduction of approximately 13% when compared to the 25% CO_2-wet system). When the proportion of CO_2-wet zones increases, the snap-off of CO_2 will be suppressed (Alyafei and Blunt, 2016; Bakhshian and Hosseini, 2019), favoring a lower trapped percentage of CO_2. The dissolution trapping capacities exhibit a similar decreasing trend when the system becomes more CO_2-wet during the CO_2 storage period. It is also essential to note the relatively small variance observed among different cases in dissolution trapping compared to that in residual entrapment. This reduction can be attributed to the limited spread of plume migration when the proportion of CO_2-wet zones increases (Fig. 12(a)), as the dissolution amount is directly dependent on the CO_2-brine contact volume. This observation indicates that dissolution trapping is also directly influenced by wettability, as it impacts the mobility of CO_2 and the migration of free CO_2 available for interaction with fresh brine.

Interestingly, there is a notable linear correlation ($R^2 > 0.99$) linking the residual/dissolution trapping capacity to the CO_2-wet fraction (Fig. 14). This correlation clearly reveals that

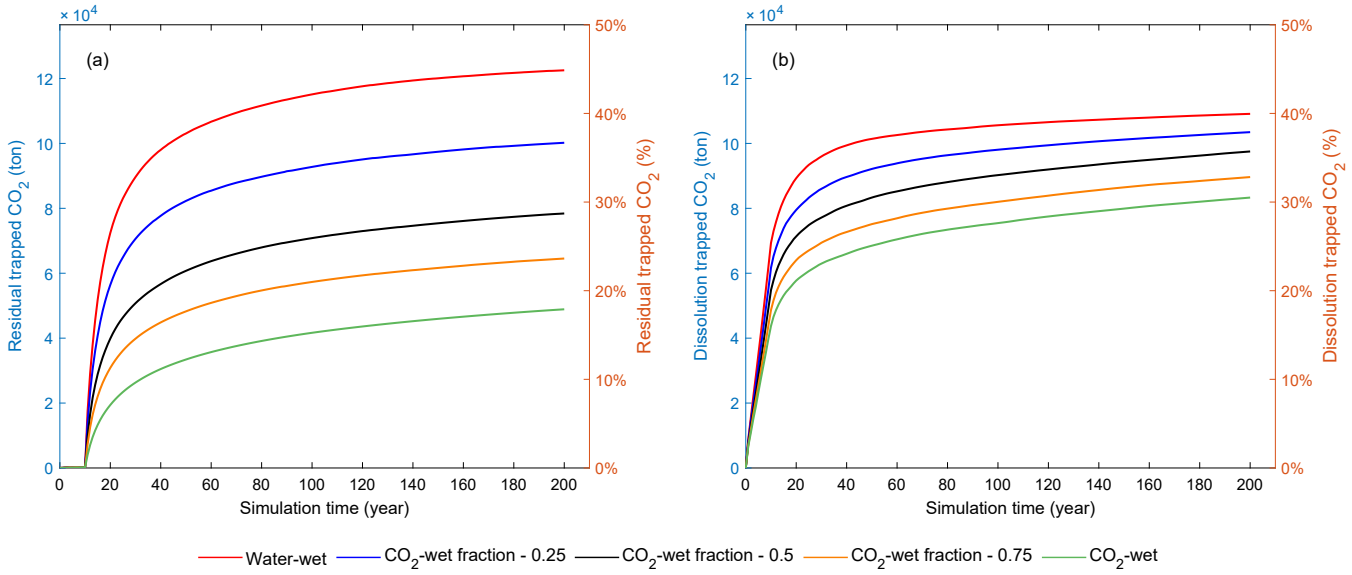

Fig. 13. (a) Residual entrapment and (b) dissolved CO_2 in different mixed-wet systems.

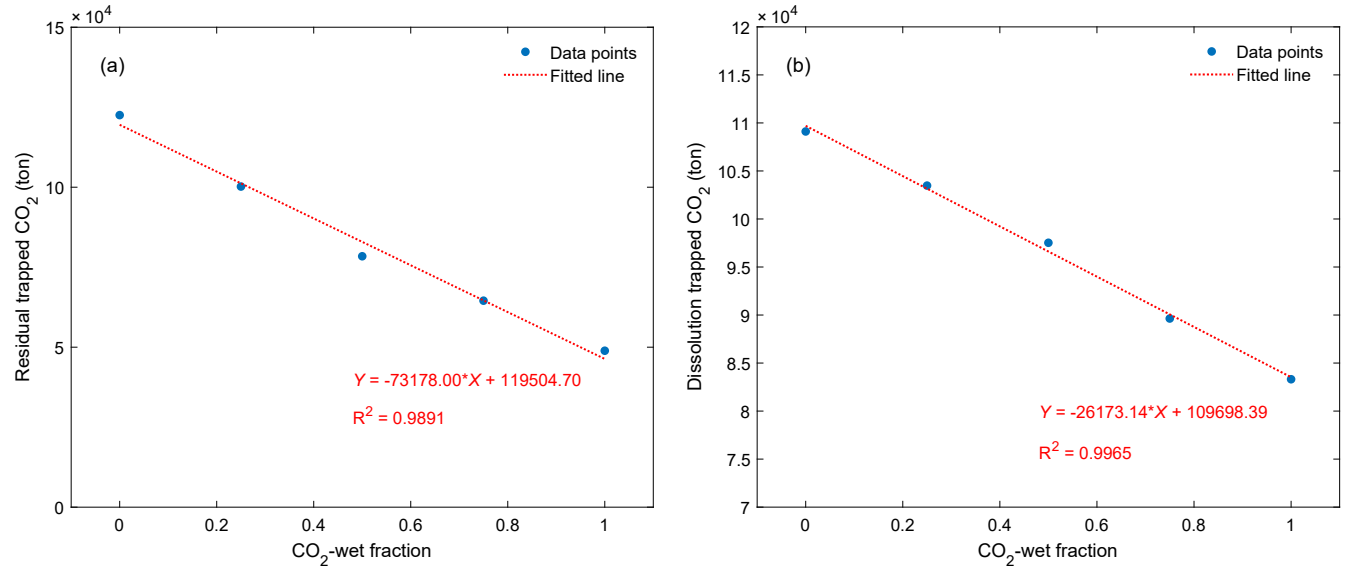

Fig. 14. Linear correlation between CO_2-wet fraction and (a) residual trapping, and (b) dissolution trapping.

the mixed-wet system has a reduced residual trapping potential compared with the water-wet system. This observation is consistent with previous experimental observations (Al-Menhali et al., 2016), where mixed-wet systems are characterized by lower residual CO_2 saturation, leading to a less pronounced residual trapping effect in comparison to water-wet systems. In water-wet systems, the residual CO_2 cluster typically follows a power-law distribution (Iglauer et al., 2013). However, a different distribution with a significantly reduced frequency of smaller clusters is observed in the mixed-wet system (Al-Menhali et al., 2016). The CO_2 as wetting phase tends to form large, interconnected ganglia in smaller pore spaces, facilitating water displacement and resulting in a lower residual CO_2 saturation, thereby leading to less significant residual trapping. Overall, a mixed-wet system with a higher fraction of CO_2-wet regions will exhibit lower trapping capacity, thereby increasing the risk of leakage.

4. Limitations and implications

Natural subsurface formations are shown to exhibit more complex wettability variations due to heterogeneous mineralogy, surface impurities, and long-term fluid-rock interactions. Our observations provide insights into the impact of such complex wettability heterogeneity (and the associated CO_2-wet fractions) on the CO_2 plume migration and trapping capacity. The general principles of reservoir modeling practices require reservoir characterization datasets and a detailed assessment of wettability regimes (e.g., random wettability distribution and

mixed-wetting implementation) can improve the predictions. More detailed modeling approaches such as incorporating multi-scale wettability datasets may refine the spatial representation of wettability heterogeneity conditions. Additionally, the geological features and structural heterogeneities such as faults, baffles, or multi-layered seal intervals, can significantly influence CO_2 flow behavior and trapping (e.g., faults and baffles act as additional barriers to enhance localized trapping). Thus, the combined effect of structural heterogeneities and wettability variations may either amplify or moderate CO_2 trapping efficiency, which should be assessed in future studies.

Our results suggest that CO_2-wet regions lead to localized high-saturation clusters due to lower gas relative permeability, while the overall residual trapping remains low. In this case, a higher injection rate may promote a more widespread CO_2 plume distribution, potentially enhancing dissolution trapping and initiating the imbibition process in new regions. However, a higher injection rate may also cause the injected CO_2 to preferentially flow through high-permeability regions, bypassing CO_2-wet zones and leading to a much rapid plume movement within the storage formation. These highlight the complex interactions between wettability, injection strategy, and CO_2 trapping mechanisms, suggesting that more detailed sensitivity analyses are needed to optimize injection parameters for long-term storage security.

5. Conclusions

This study investigated the influence of internal wettability variations in a single formation model on plume movement and the trapping efficiency for large-scale CO_2 storage in saline aquifers. To this end, different wettability-dependent trapping coefficients were assigned to different locations of the formation to represent the local wetting characteristics. Different water-wet systems, including uniform strongly water-wetting, heterogeneous water-wetting, and uniform weakly water-wetting, were designed for comparisons. In the internal wettability heterogeneity cases, the CO_2 accumulated area exhibits more compact and constrained patterns compared with the weakly water-wet systems. The local wettability variations also result in a more complex localized imbibition process, leading to pronounced variations in local residual CO_2 saturation. The residual trapping capacity also experiences an approximately 35% reduction and an approximately 20% enhancement in the wettability heterogeneity cases compared to uniform strongly water-wet and uniform less water-wet systems, respectively. This indicates that trapping potential estimation based on uniform wettability assumption will lead to overestimations/underestimations.

Moreover, in the overall water-wet cases considering both residual and dissolution trapping mechanisms, the residual and dissolution trapping capacity of the heterogeneous wettability system fall between the capacities of the two single wettability systems. Different wettability distribution patterns (i.e., random and normal) result in slightly different residual trapping capacities with comparable dissolution trapping capacities.

In a mixed-wet system, plume migration and residual CO_2 saturation vary notably with CO_2-wet fraction. Lower CO_2-wet fraction promotes widespread plume distribution and higher residual gas saturation, while high CO_2-wet fraction leads to localized concentrations and significantly lower residual CO_2 saturation. This further leads to a decrease in both residual and dissolution trapping when the proportion of CO_2-wet zones increases. Our findings also indicate that there is a strong linear correlation ($R^2 > 0.99$) between the CO_2-wet fraction and the residual/dissolution trapping capacity.

Overall, our findings clearly suggest that the internal wettability variations of saline aquifers introduce greater bias or unpredictability in terms of trapping potential and dynamics of plume migration - thus the consideration of non-uniform wettability in field-scale predictions is imperative. The results of this study represent more realistic formation wettability conditions, thus providing insights for mitigating risks associated with large-scale CO_2 storage in saline aquifers.

Supplementary file

https://doi.org/10.46690/ager.2025.03.06

Conflict of interest

The authors declare no competing interest.

References

Ali, M., Awan, F. U. R., Ali, M., et al. Effect of humic acid on CO_2-wettability in sandstone formation. Journal of Colloid and Interface Science, 2021, 588: 315-325.

Al-Khdheeawi, E. A., Vialle, S., Barifcani, A., et al. Impact of reservoir wettability and heterogeneity on CO_2-plume migration and trapping capacity. International Journal of Greenhouse Gas Control, 2017, 58: 142-158.

Al-Khdheeawi, E. A., Vialle, S., Barifcani, A., et al. Effect of wettability heterogeneity and reservoir temperature on CO_2 storage efficiency in deep saline aquifers. International Journal of Greenhouse Gas Control, 2018, 68: 216-229.

Al-Menhali, A. S., Krevor, S. Capillary trapping of CO_2 in oil reservoirs: Observations in a mixed-wet carbonate rock. Environmental Science & Technology, 2016, 50(5): 2727-2734.

Al-Menhali, A. S., Menke, H. P., Blunt, M. J., et al. Pore scale observations of trapped CO_2 in mixed-wet carbonate rock: Applications to storage in oil fields. Environmental Science & Technology, 2016, 50(18): 10282-10290.

Al-Naimi, K., Arif, M., Aboushanab, M., et al. Micro-scale wettability of carbonate rocks via high-resolution ESEM imaging. Results in Physics, 2023, 52: 106871.

Alyafei, N., Blunt, M. J. The effect of wettability on capillary trapping in carbonates. Advances in Water Resources, 2016, 90: 36-50.

Andrew, M., Bijeljic, B., Blunt, M. J. Pore-scale contact angle measurements at reservoir conditions using X-ray microtomography. Advances in Water Resources, 2014,

68: 24-31.

Arif, M., Abu-Khamsin, S. A., Iglauer, S. Wettability of rock/CO_2/brine and rock/oil/CO_2-enriched-brine systems: Critical parametric analysis and future outlook, Advances in Colloid and Interface Science, 2019, 268: 91-113.

Arif, M., Awan, F. U. R., Zhang, H., et al. Coal wettability: A holistic overview of the data sets, influencing factors, and knowledge gaps. Energy & Fuels, 2024, 38(16): 15069-15084.

Arjomand, E., Myers, M., Al Hinai, N. M., et al. Modifying the wettability of sandstones using nonfluorinated silylation: To minimize the water blockage effect. Energy & Fuels, 2020, 34(1): 709-719.

Bachu, S. Drainage and imbibition CO_2/brine relative permeability curves at *in situ* conditions for sandstone formations in western Canada. Energy Procedia, 2013, 37: 4428-4436.

Bakhshian, S., Hosseini, S. A. Pore-scale analysis of supercritical CO_2-brine immiscible displacement under fractional-wettability conditions. Advances in Water Resources, 2019, 126: 96-107.

Basirat, F., Yang, Z., Niemi, A. Pore-scale modeling of wettability effects on CO_2-brine displacement during geological storage. Advances in Water Resources, 2017, 109: 181-195.

Blunt, M. J., Lin, Q., Akai, T., et al. A thermodynamically consistent characterization of wettability in porous media using high-resolution imaging. Journal of Colloid and Interface Science, 2019, 552: 59-65.

Chang, C., Kneafsey, T. J., Wan, J., et al. Impacts of mixed-wettability on brine drainage and supercritical CO_2 storage efficiency in a 2.5-D heterogenaeous micromodel. Water Resources Research, 2020, 56(7): e2019WR026789.

Ershadnia, R., Singh, M., Mahmoodpour, S., et al. Impact of geological and operational conditions on underground hydrogen storage. International Journal of Hydrogen Energy, 2023, 48(4): 1450-1471.

Floris, F. J. T., Bush, M. D., Cuypers, M., et al. Methods for quantifying the uncertainty of production forecasts: A comparative study. Petroleum Geoscience, 2001, 7(S): S87-S96.

Hu, R., Wan, J., Kim, Y., et al. Wettability effects on supercritical CO_2-brine immiscible displacement during drainage: Pore-scale observation and 3D simulation. International Journal of Greenhouse Gas Control, 2017, 60: 129-139.

Iglauer, S., Al-Yaseri, A. Improving basalt wettability to de-risk CO2 geo-storage in basaltic formations. Advances in Geo-Energy Research, 2021, 5(3): 347-350.

Iglauer, S., Paluszny, A., Blunt, M. J. Simultaneous oil recovery and residual gas storage: A pore-level analysis using *in situ* X-ray micro-tomography. Fuel, 2013, 103: 905-914.

Juanes, R., Spiteri, E. J., Orr, F. M., et al. Impact of relative permeability hysteresis on geological CO_2 storage. Water Resources Research, 2006, 42(12): W12418.

Khishvand, M., Alizadeh, A. H., Piri, M. *In-situ* characterization of wettability and pore-scale displacements during two- and three-phase flow in natural porous media. Advances in Water Resources, 2016, 97: 279-298.

Krevor, S., Blunt, M. J., Benson, S. M., et al. Capillary trapping for geologic carbon dioxide storage-From pore scale physics to field scale implications. International Journal of Greenhouse Gas Control, 2015, 40: 221-237.

Krevor, S., De Coninck, H., Gasda, S. E., et al. Subsurface carbon dioxide and hydrogen storage for a sustainable energy future. Nature Reviews Earth & Environment, 2023, 4(2): 102-118.

Lv, P., Liu, Y., Wang, Z., et al. In situ local contact angle measurement in a CO_2-brine-sand system using microfocused X-ray CT. Langmuir, 2017, 33(14): 3358-3366.

Niu, B., Al-Menhali, A., Krevor, S. C. The impact of reservoir conditions on the residual trapping of carbon dioxide in Berea sandstone. Water Resources Research, 2015, 51(4): 2009-2029.

Øren, P. E., Ruspini, L. C., Saadatfar, M., et al. *In-situ* pore-scale imaging and image-based modelling of capillary trapping for geological storage of CO_2. International Journal of Greenhouse Gas Control, 2019, 87: 34-43.

Rahman, T., Lebedev, M., Barifcani, A., et al. Residual trapping of supercritical CO_2 in oil-wet sandstone. Journal of Colloid and Interface Science, 2016, 469: 63-68.

Safi, N., Rashid, M., Shakoor, U., et al. Understanding the role of energy productivity, eco-innovation and international trade in shaping consumption-based carbon emissions: A Study of BRICS nations. Environmental Science and Pollution Research, 2023, 30(43): 98338-98350.

Wang, S., Tokunaga, T. K. Capillary pressure-saturation relations for supercritical CO_2 and brine in limestone/-dolomite sands: Implications for geologic carbon sequestration in carbonate reservoirs. Environmental Science & Technology, 2015, 49(12): 7208-7217.

Wei, B., Wang, B., Li, X., et al. CO2 storage in depleted oil and gas reservoirs: A review. Advances in Geo-Energy Research, 2023, 9(2): 76-93.

Wang, Y., Wang, J., Liu, H., et al. Effects of acid–rock reaction on physical properties during CO2-rich industrial waste gas (CO_2-rich IWG) injection in shale reservoirs. Petroleum Science, 2024, 21(1): 272-285.

Zhang, H., Al Kobaisi, M., Arif, M. Impact of wettability and injection rate on CO_2 plume migration and trapping capacity: A numerical investigation. Fuel, 2023, 331: 125721.

Zhang, H., Arif, M. Residual trapping capacity of subsurface systems for geological storage of CO_2: Measurement techniques, meta-analysis of influencing factors, and future outlook. Earth-Science Reviews, 2024: 104764.

Zhang, H., Zhang, Y., Arif, M. CO_2 geological storage in subsurface aquifers as a function of brine salinity: A field-scale numerical investigation. Geoenergy Science and Engineering, 2025, 245: 213505.